# Large-signal Stability Analysis of Inverter-based Microgrids via Sum of Squares Technique

1<sup>st</sup> Hadis Hosseinpour, 2<sup>nd</sup> Mohammad MansourLakouraj, 3<sup>rd</sup> Mohammed Ben-Idris, 4<sup>th</sup> Hanif Livani Department Electrical & Biomedical Engineering, University of Nevada, Reno, Reno, NV, US 1<sup>st</sup> hhosseinpour@unr.edu, 2<sup>nd</sup> mansour@nevada.unr.edu, 3<sup>rd</sup> mbenidris@unr.edu, 4<sup>th</sup> hlivani@unr.edu

Abstract—Increasing the penetration of low inertia inverterbased resources in power systems creates new system stability challenges and requires sophisticated stability assessment tools. One of the practical tools for large-signal stability assessment is determining the system region of stability (ROS)—i.e., the portion of the system state space where variable trajectories converge to a stable equilibrium point. In contrast to time-domain simulation methods, Lyapunov function-based methods are fast and can measure system stability margin from the ROS. This paper proposes a sum of squares (SOS) technique to determine large-signal stability regions of inverter-based microgrids using the Lyapunov function. An accurate dynamic model of grid-connected inverterbased resources is applied for the state-space model of the network. The Lyapunov function is constructed based on the sum of squares method by SOSTOOL. In comparison to Krasovskii's method, the stability region created by the SOS method is found more accurate. Two scenarios—a changing load event and an adjustment to the inverter control—are analyzed in the stability region assessment.

Index Terms—Inverter-based resources, large-signal stability, Lyapunov function, the sum of squares method, the domain of attraction.

### I. INTRODUCTION

Enhancing the resilience, dependability, and flexibility of the power supply is the primary factor behind the development and deployment of microgrids, generally known as small-scale autonomous energy systems [1]. Utilizing microgrids can help lower operating expenses and improve the integration of renewable energy sources [2]. However, because of their low inertia, microgrid applications create stability problems. In order to use microgrids as practical energy systems for enhancing the resilience, reliability, and flexibility of the power supply, stability assessment of low-inertia microgrids is crucial.

Both small-signal and large-signal models have been used to study and analyze the stability of microgrids [3]. Applying linearization techniques on the system dynamic model around the equilibrium point or operating point of the power grid (i.e., small-signal stability) analysis exclusively small transient disruptions [4]. Therefore, to guarantee a comprehensive stability assessment, a large-signal stability analysis must be carried out for significant disturbances including line failures, faults, and load changes.

One of the promising methods to evaluate large-signal stability assessment of microgrids is the Lyapunov-based technique [5]. The Lyapunov stability assessment can properly define the stability boundary for nonlinear systems. Due to the

significant portion of non-linear components of inverter-based microgrids, detailed models are required for precise large-signal stability analysis. Applying Lyapunov-based methods with intricate component models has shown to be a challenge for the stability assessment of large-scale power systems.

For the stability evaluation and control of single components such as motor drives, rectifiers, and inverters, Lyapunov techniques have been employed extensively. Large-signal stability analysis of a single inverter-motor drive system in a DC power system is evaluated in [6]. In [7], the stability assessment of a microgrid including three inverter-based resources under different events is investigated using Krasovskii's method. An inverter-based generator's large-signal stability is investigated in [8], by utilizing a Popov-based Lyapunov function. However, the domain of attraction obtained by the Popov-based Lyapunov function is conservative. Moreover, other methods such as those using Krasovskii's method suffer from the same conservativeness problem.

The small domain of attraction which is the result of using conservative methods makes the protection setting conservative against possible faults and contingencies, leading to the quick tripping of the protection system. Subsequently, the system experiences an unnecessary outage that can cause customer inconvenience and shortages of supply. To circumvent the conservativeness challenge, the sum of squares method [9] can be used for stability analysis, providing a larger provable domain of attraction for the same system compared to the previous methods like Popove and Krasovskii's method.

In this study, the sum of squares (SOS) method is applied on a microgrid for the stability analysis to estimate a less conservative domain of attraction. In this study:

- The sum of squares method is applied to the time-domain dynamic model of a microgrid to construct the Lyapunov function and estimate a less conservative stability region.
- The domain of attraction constructed by the sum of squares and Krasovskii's methods are comparatively studied
- The effect of two scenarios including inverter control modification and load-changing event on the SOS-based domain of attraction are scrutinized.

The contour plot tool is applied to present the results.

The rest of the paper is structured as follows. Section II presents the nonlinear dynamic model of a grid-connected microgrid. Section III explains the sum of squares method

for constructing the Lyapunov function. Section IV provides case study results and their assessment. Concluding remarks are included in Section V.

# II. DYNAMIC MODEL OF A GRID-CONNECTED MICROGRID

A microgrid's large-signal dynamic model is applied to investigate the system's dynamic response against various extreme contingencies and disruptions. All components of a distribution system, such as distributed generators (DGs), converters, loads, and batteries, should be modeled using reasonable approximations to obtain a precise large-signal model of the microgrid.

Fig. 1 represents the network and the controlling system of the inverter-based resource studied in this paper. The Network includes an inverter-based resource connected to the main grid and two loads. In this study, the dynamic model of the inverter-based resource is as the proposed model in [5], [10]. The following subsections describe the inverterbased resource's theoretical model. The power control, voltage control, current control, LCL filter, lines and connection, and loads are modeled and presented. In the end, all components using the network mapping model are combined to construct the state space model of the microgrid. In this model, the DC side components are ignored.

a) Power Controller: The power controller includes Q/V, P/f, and low-pass filter  $(\omega_f)$ . The nonlinear state-space model of the power controller is as follows:

$$P_{i} = \frac{\omega_{f}}{s + \omega_{f}} \tilde{p} \qquad , \quad Q_{i} = \frac{\omega_{f}}{s + \omega_{f}} \tilde{q}$$

$$\tilde{p} = v_{oq} i_{oq} + v_{od} i_{od} \quad , \quad \tilde{q} = v_{od} i_{oq} - v_{oq} i_{od}$$

$$(1)$$

$$m_p P_i = \omega_n - \omega , \quad n_q Q_i = V_n - v_{od}^* , \quad v_{oq}^* = 0$$

$$\delta = \int (\omega - \omega_{ref}) \quad , \quad \triangle \omega_n = \omega_n - \omega_{ref}$$
(2)

$$\begin{split} \dot{X}_{P_{ctrl}} = & \mathbf{A_{P}} \ X_{P_{ctrl}} + \mathbf{B_{P}} \omega \ \triangle \omega_{n} + \mathbf{B_{P}} \ U_{inv} \\ Y_{P_{ctrl}} = & \mathbf{C_{P}} \ X_{P_{ctrl}} + \mathbf{E_{P}} \\ X_{P_{ctrl}}^{T} = & \begin{bmatrix} \delta & P & Q \end{bmatrix}, Y_{P_{ctrl}}^{T} = \begin{bmatrix} \omega & v_{od}^{*} & v_{oq}^{*} \end{bmatrix}, \\ U_{inv}^{T} = & \begin{bmatrix} i_{ld} & i_{lq} & v_{od} & v_{oq} & i_{od} & i_{oq} \end{bmatrix}, \mathbf{E_{P}} = \begin{bmatrix} \omega_{n} \\ V_{n} \\ 0 \end{bmatrix}, \end{split}$$

where  $P_i$  and  $Q_i$  are considered P and Q, respectively. The angle between the inverter's local d-q reference frame and the global D-Q reference frame is represented by  $\delta$ .  $V_n$  indicates d-axis nominal output voltage, and  $\omega_n$  represents the nominal

frequency is set in the inverter droop controller; and  $\omega$  and  $\omega_{ref}$  are local rotating reference frame of each inverter and angular frequencies of the global reference frame, respectively.

b) Voltage Controller: Following is a definition of the voltage controller's state space:

$$\frac{\mathrm{d}\zeta_d}{\mathrm{d}t} = v_{od}^* - v_{od}, \quad \frac{\mathrm{d}\zeta_q}{\mathrm{d}t} = v_{oq}^* - v_{oq} \tag{5}$$

$$\dot{X}_{V_{ctrl}} = \mathbf{A_v} X_{V_{ctrl}} + \mathbf{B_{v1}} U_v + \mathbf{B_{v2}} U_{inv} 
Y_{V_{ctrl}} = \mathbf{C_v} X_{V_{ctrl}} + \mathbf{D_{v1}} U_v + \mathbf{D_{v2}} U_{inv}$$
(6)

$$\begin{split} X_{\zeta_{ctrl}} &= \begin{bmatrix} \zeta_d \\ \zeta_q \end{bmatrix}, \, Y_{\zeta_{ctrl}} = \begin{bmatrix} i_{ld}^* \\ i_{lq}^* \end{bmatrix}, \, U_v = \begin{bmatrix} v_{od}^* \\ v_{oq}^* \end{bmatrix}, \\ \mathbf{B_{v1}} &= \begin{bmatrix} 1 & 0 \\ 0 & 1 \end{bmatrix}, \, \mathbf{B_{v2}} = \begin{bmatrix} 0 & 0 & -1 & 0 & 0 & 0 \\ 0 & 0 & 0 & -1 & 0 & 0 \end{bmatrix}, \\ \mathbf{A_{v}} &= \begin{bmatrix} 0 & 0 \\ 0 & 0 \end{bmatrix}, \, \mathbf{C_{v}} &= \begin{bmatrix} K_{iv} & 0 \\ 0 & K_{iv} \end{bmatrix}, \, \mathbf{D_{v1}} = \begin{bmatrix} K_{pv} & 0 \\ 0 & K_{pv} \end{bmatrix}, \\ \mathbf{D_{v2}} &= \begin{bmatrix} 0 & 0 & -K_{pv} & -\omega_n \, C_f & F & 0 \\ 0 & 0 & \omega_n \, C_f & -K_{pv} & 0 & F \end{bmatrix} \end{split}$$

$$(7)$$

where the Proportional Integral (PI) coefficients of the voltage controller of the inverter are represented by  $K_{pv}$  and  $K_{iv}$ . Additionally, F indicates the feed-forward coefficient of the voltage controller of the inverter. In this study, the microgrid is assumed to operate in the grid-connected mode, and the grid frequency is set as the angular frequency of the global D-Q reference frame.

c) Current Controller: The state space model of the current controller is as follows.

$$\frac{\mathrm{d}\gamma_d}{\mathrm{d}t} = i_{ld}^* - i_{ld}, \quad \frac{\mathrm{d}\gamma_q}{\mathrm{d}t} = i_{lq}^* - i_{lq}$$
 (8)

$$\dot{X}_{\gamma_{ctrl}} = \mathbf{A_c} X_{\gamma_{ctrl}} + \mathbf{B_{c1}} U_c + \mathbf{B_{c2}} U_{inv} 
Y_{\gamma_{ctrl}} = \mathbf{C_c} X_{\gamma_{ctrl}} + \mathbf{D_{c1}} U_c + \mathbf{D_{c2}} U_{inv}$$
(9)

where  $K_{ic}$  and  $K_{pc}$  are the current controller's PI coefficients.

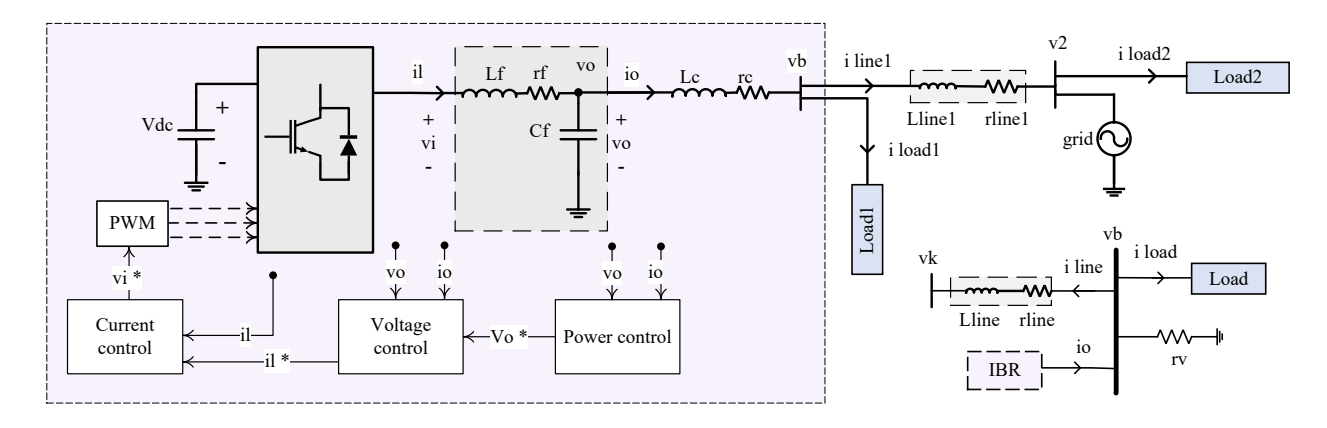


Fig. 1. Network and the DC/AC droop controlled inverter.

(12)

d) LCL Filter: The LC filter can be modeled as follows:

$$\frac{\mathrm{d}i_{ld}}{\mathrm{d}t} = \frac{-r_f}{L_f} i_{ld} + \omega i_{lq} + \frac{1}{L_f} \left( v_{inv,d} - v_{od} \right) 
\frac{\mathrm{d}i_{lq}}{\mathrm{d}t} = \frac{-r_f}{L_f} i_{lq} - \omega i_{ld} + \frac{1}{L_f} \left( v_{inv,q} - v_{oq} \right) 
\frac{\mathrm{d}v_{od}}{\mathrm{d}t} = \omega v_{oq} + \frac{1}{C_f} \left( i_{ld} - i_{od} \right) 
\frac{\mathrm{d}v_{oq}}{\mathrm{d}t} = -\omega v_{od} + \frac{1}{C_f} \left( i_{lq} - i_{oq} \right) 
\frac{\mathrm{d}i_{od}}{\mathrm{d}t} = \frac{-r_c}{L_c} i_{od} + \omega i_{oq} + \frac{1}{L_c} \left( v_{od} - v_{bd} \right) 
\frac{\mathrm{d}i_{oq}}{\mathrm{d}t} = \frac{-r_c}{L_c} i_{oq} - \omega i_{od} + \frac{1}{L_c} \left( v_{oq} - v_{bq} \right) 
\dot{X}_{LC_{fltr}} = \mathbf{A_{LC}} X_{LC_{fltr}} + \mathbf{B_{LC1}} U_{LC1} + \mathbf{B_{LC2}} U_{LC2} 
X_{LC_{fltr}} = U_{inv}, U_{LC1} = \begin{bmatrix} v_{inv,d} \\ v_{inv,q} \end{bmatrix}, U_{LC2} = \begin{bmatrix} v_{bd} \\ v_{bq} \end{bmatrix}$$

where  $v_{bd}$  and  $v_{bq}$  are the output voltage in Park frame, and  $A_{LC}$ ,  $B_{LC1}$ , and  $B_{LC2}$  are explained in [5].

e) State-Space model of an Inverter-based Resource: The three-phase system has no harmonics and is balanced. In this study, the modulation ratio is assumed equal to 1. According to [5], for the state-space model of an inverter-based resource, all aforementioned dynamic model equations are combined as follows:

$$\dot{X}_{IBR} = \mathbf{A}_{IBR} X_{IBR} + \mathbf{B}_{IBR1} U_{IBR} + \mathbf{B}_{IBR2} + \mathbf{B}_{IBR3} \omega_{ref}$$

$$Y_{IBR} = \mathbf{C}_{IBR} X_{IBR} + \mathbf{D}_{IBR1} \omega_{n}$$

$$X_{IBR}^{T} = \begin{bmatrix} \delta & P & Q & \zeta_{d} & \zeta_{q} & \gamma_{d} & \gamma_{q} & i_{ld} & i_{lq} & v_{od} & v_{oq} \\ & & & & & & & & \\ & & & & & & & \\ & & & & & & & \\ & & & & & & & \\ & & & & & & & \\ & & & & & & \\ & & & & & & \\ & & & & & & \\ & & & & & & \\ & & & & & & \\ & & & & & & \\ & & & & & & \\ & & & & & & \\ & & & & & \\ & & & & & & \\ & & & & & \\ & & & & & \\ & & & & & \\ & & & & & \\ & & & & & \\ & & & & & \\ & & & & & \\ & & & & & \\ & & & & & \\ & & & & & \\ & & & & \\ & & & & \\ & & & & \\ & & & & \\ & & & & \\ & & & & \\ & & & & \\ & & & & \\ & & & & \\ & & & & \\ & & & & \\ & & & & \\ & & & & \\ & & & & \\ & & & & \\ & & & \\ & & & & \\ & & \\ & & & \\ & & \\ & & & \\ & & & \\ & & \\ & & & \\ & & \\ & & \\ & & & \\$$

where  $A_{IBR}$ ,  $B_{IBR2}$ , and  $D_{IBR}$  are given in (14); in (14),  $C'_P$  is the rows 2 and 3 of  $C_P$ , which is given in (4). The other parameters, including  $B_{IBR1}$ ,  $B_{IBR3}$ , and  $C_{IBR}$  can be found in [5], [10].

f) Network: The dynamic equation of the network is as follows:

$$\frac{\mathrm{d}i_{D,line}}{\mathrm{d}t} = \frac{-r_{line} i_{D,line}}{L_{line}} - \frac{(v_{kD} - v_{bD})}{L_{line}} + \omega i_{Q,line} 
\frac{\mathrm{d}i_{Q,line}}{\mathrm{d}t} = \frac{-r_{line} i_{Q,line}}{L_{line}} - \frac{(v_{kQ} - v_{bQ})}{L_{line}} - \omega i_{D,line}$$
(15)

The nonlinear state-space model of the network is given by:

$$\dot{X}_{i_{Ntwrk}} = \mathbf{A}_{\mathbf{Ntwrk}} X_{i_{Ntwrk}} + \mathbf{B}_{\mathbf{Ntwrk}} U_{Ntwrk}$$
 (16)

$$X_{i_{Ntwrk}}^{T} = \begin{bmatrix} X_{i_{line1}}^{T} \end{bmatrix}, U_{Ntwrk}^{T} = \begin{bmatrix} v_{bDQ1}^{T} & v_{bDQ2}^{T} \end{bmatrix},$$

$$X_{i_{line}} = \begin{bmatrix} i_{D,line} \\ i_{Q,line} \end{bmatrix}, \quad v_{bDQ} = \begin{bmatrix} v_{bD} \\ v_{bQ} \end{bmatrix}$$

$$\mathbf{A}_{\mathbf{Ntwrk}} = \begin{bmatrix} A_{LINE1} \end{bmatrix},$$

$$\mathbf{A}_{\mathbf{LINE1}} = \begin{bmatrix} -r_{line}/L_{line} & \omega_{ref} \\ -\omega_{ref} & -r_{line}/L_{line} \end{bmatrix},$$

$$\mathbf{B}_{\mathbf{Ntwrk}}^{\mathbf{T}} = \begin{bmatrix} B_{LINE1}^{T} \end{bmatrix},$$

$$\mathbf{B}_{\mathbf{LINE1}} = \begin{bmatrix} \frac{1}{L_{line}} & 0 & \frac{-1}{L_{line}} & 0 \\ 0 & \frac{1}{L_{line}} & 0 & \frac{-1}{L_{line}} \\ 0 & \frac{-1}{L_{line}} \end{bmatrix},$$

$$-node\ b - -node\ k -$$

where the network topology and line config are represented by the variables  $(.)_{Ntwrk}$  and  $(.)_{LINE}$ , respectively.; and  $v_k$  and  $v_b$  are defined  $v_{b2}$  (or  $v_2$ ) and  $v_{b1}$  based on the Fig. 1. In matrix  $\mathbf{B_{LINE}}$ , the line current leaves the node b (+1/ $L_{line}$ ) and enters to the node k (-1/ $L_{line}$ ). The other components of this matrix have values of zero.

g) **Load**: In this study, a general constant resistiveinductive (RL) load type is considered. The load dynamics behavior at each node is modeled as follows:

$$\frac{\mathrm{d}i_{D,load}}{\mathrm{d}t} = \frac{-R_{load} i_{D,load}}{L_{load}} + \frac{v_{bD}}{L_{load}} + \omega i_{Q,load} 
\frac{\mathrm{d}i_{Q,load}}{\mathrm{d}t} = \frac{-R_{load} i_{Q,load}}{L_{load}} + \frac{v_{bQ}}{L_{load}} - \omega i_{D,load}$$
(18)

$$\dot{X}_{i_{load}} = \mathbf{A_{load}} \, X_{i_{load}} + \mathbf{B_{load}} \, U_{load}$$

$$X_{i_{load}} = \begin{bmatrix} i_{D,load} \\ i_{Q,load} \end{bmatrix}, U_{load} = U_{LC2} [T_{DQ}] = \begin{bmatrix} v_{bD} \\ v_{bQ} \end{bmatrix},$$

$$\mathbf{A_{load}} = \begin{bmatrix} -R_{load}/L_{load} & \omega_{ref} \\ -\omega_{ref} & -R_{load}/L_{load} \end{bmatrix},$$

$$\mathbf{B_{load}} = \begin{bmatrix} 1/L_{load} & 0 \\ 0 & 1/L_{load} \end{bmatrix}$$
(19)

where  $T_{DQ}$  is the transfer function for the global D-Q reference frame

h) Microgrid Model and Mapping matrices: To determine the voltage of each node, a virtual resistor  $(r_v)$  is provided between the ground and each node. In Fig. 1, the virtual resistor is depicted, where a large enough amount is chosen for it  $(7000 \ \Omega)$ , minimizing its effect on the grid's dynamic model's precision. The voltage of nodes is expressed as follows:

$$v_{bDQ} = \mathbf{R_v} (\mathbf{M_{IBR}} \ i_{oDQ} + \mathbf{M_L} \ i_{loadDQ} + \mathbf{M_{Ntwrk}} \ i_{lineDQ})$$
(20)

The voltage values given in (20) are then used as the input of load (L), line (Network), and inverter (IBR) models.  $R_v$  is the matrix of  $r_v$  based on the configuration and number of nodes.  $\mathbf{R_v}$  contains diagonal items with the value  $r_v$ .  $\mathbf{M_{IBR}}$  is intended to map the inverters' connecting points to the grid's nodes. Depending on whether the inverter i is linked to the node j, the corresponding element is either 1 or 0. The connection between loads and grid nodes is mapped using  $\mathbf{M_L}$ . In the absence of a connection between the load and the node, the element is 1, otherwise, it is 0. The mapping of the lines to the nodes of the grid is done by item  $\mathbf{M_{Ntwrk}}$ . This matrix's element has a value of 1 when the current enters the node and a value of -1 when it exits [5], [10]. The following is a description of the state-space model for all components [5].

$$\dot{X}_{Microgrid} = \mathbf{A}_{\mathbf{Microgrid}} (\mathbf{X}_{\mathbf{Microgrid}}) X_{Microgrid} + \mathbf{B}_{\mathbf{Microgrid}}$$
(21)

where  $A_{Microgrid}$  is presented in (22) and additional information about the matrices of (22) is available in [10] (Section II-B, Eq. 52).

# III. CONSTRUCTING THE LYAPUNOV FUNCTION BY SOSTOOL

In Parrilo's thesis, the sum of squares method was first presented [11]. In this method, numerous problems in system

analysis that were previously challenging to answer have been addressed. One of the addressed challenges is the algorithmic stability analysis of nonlinear systems using Lyapunov techniques. In this paper, the application of the SOS-based Lyapunov function is suggested for stability analysis of the inverter-based microgrid to find a region of attraction with lower conservativeness. The SOSTOOL is applied to find the polynomial Lyapunov function. The sum of squares polynomial optimization programs can be created and solved using the free MATLAB toolbox SOSTOOLS [12]. According to the number of states in the inverter-based resource model, the constructed Lyapunov function by SOSTOOL is too bulky to present here.

#### IV. RESULTS AND ANALYSIS

The case study includes two loads and an inverter-based resource connected to the main grid. The parameter of the network is tabulated in Table I. The stability analysis is comparatively discussed for both SOS-based Lyapunov function and Krasovoskii's methods. The sensitivity analysis of the SOS-based method is investigated for two scenarios including load changing and control parameter modifications. In this study, the contour plot is used to represent the results.

TABLE I
THE PARAMETERS OF THE INVERTER CONTROL AND NETWORK

$K_{pv}$	0.225	$L_f$	10.1 mH	$m_p$	8.9e-5
$K_{iv}$	610	$C_f$	$6600~\mu F$	$n_q$	2.5e-3
$K_{pc}$	63	$r_f$	0.1 Ω	$\omega_{ref}$	$2 \times 50 \pi \ rad/s$
$K_{ic}$	1620	$V_n$	380.5 volt	$\omega_f$	$2\times5\pi \ rad/s$

A contour plot is a graphical technique for portraying a three-dimensional area that involves drawing contours on a two-dimensional platform using constant z-slice data. In other words, assuming a value for z value, lines are created linking the (x,y) places where that value of z occurs. The number on the contour line shows the z value. Moreover, the changing color between each two contour lines shows the different z-slices.

# A. Accuracy of the SOS-based Stability Region

As claimed about the accuracy of the SOS-based Lyapunov function, this method can enlarge the domain of attraction to provable state space. Fig. 2 represents a comparative study for the domain of attraction constructed by two methods including Krasovskii and the sum of squares. The stable

$$A_{IBR} = \begin{bmatrix} A_{P} & 0_{3\times4} & B_{P} \\ B_{v1} C'_{P} & 0_{2\times4} & B_{v2} \\ B_{c1} D_{v1} C'_{P} & B_{c1} C_{v} & 0_{2\times2} & B_{c1} D_{v2} + B_{c2} \\ \psi B_{LCL1} D_{c1} D_{v1} C'_{P} & \psi B_{LCL1} D_{c1} C_{v} & \psi B_{LCL1} C_{c} & \sigma \end{bmatrix}_{13\times13}$$
(14)  
$$\psi = G_{IBR} V_{dc} , \quad \sigma = A_{LCL} + B_{LCL1} \psi \left( D_{c1} D_{v2} + D_{c2} \right) ,$$
$$D_{IBR}^{T} = \begin{bmatrix} 1 & 0_{1\times2} \end{bmatrix}, \quad B_{IBR2}^{T} = \begin{bmatrix} \omega_{n} & 0_{1\times2} & V_{n} & 0 & K_{pv} V_{n} & 0_{1\times7} \end{bmatrix}$$

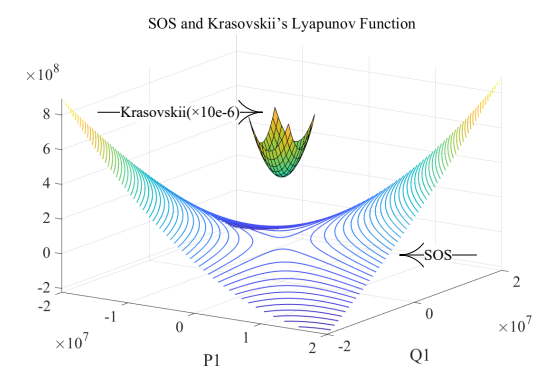


Fig. 2. (a) Domain of attraction based on SOS (contour) and Krasovskii(surf).

state space represented by Krasovskii's method is extremely small compared to what is constructed by the sum of squares method. The domain of attraction proposed by Krasovskii causes a very conservative response of the power system during the contingencies. Generally, the relay and protection systems are adjusted based on the transient stability analysis like the domain of attraction. The domain of attraction can determine the critical time to clear the fault and other contingencies to guarantee a stable and reliable operation of the network. A small domain of attraction leads to a conservative adjustment of the protection system, and as a result, the system experiences an excessive outage or load shedding.

# B. Analysis of the Region of Stability using Contour Plot

Based on the Lyapunov stability, the constructed Lyapunov function must have the following conditions for the stability region:

$$V(0) = 0$$
,  $V(x_n) > 0$ ,  $\dot{V}(x_n) \le 0$  (23)

For the first condition, the state space of the system is shifted to its equilibrium point (i.e.  $x_n = x - x_0$  that  $x_0$  is the equilibrium point of the system). So,  $V(x_n)$  at  $x_n = 0$  is zero. Fig. 3 illustrates the Lyapunov function (left) and the derivative of the Lyapunov function (right). Negative contours in the Lyapunov function plot cannot satisfy the second Lyapunov stability condition. As a result, the regions in Fig. 3-(left) with dark purple areas are not included in the stability region. The positive contours in Fig. 3-(right), which include the yellow and light orange zones, are excluded from the stability region, satisfying the third criterion for the negative derivative of the Lyapunov function. Consequently, the common area of the second and third conditions constructs the stability region. In Fig. 4, red lines created as a result of subscribing to the second and third conditions identify the stability region.

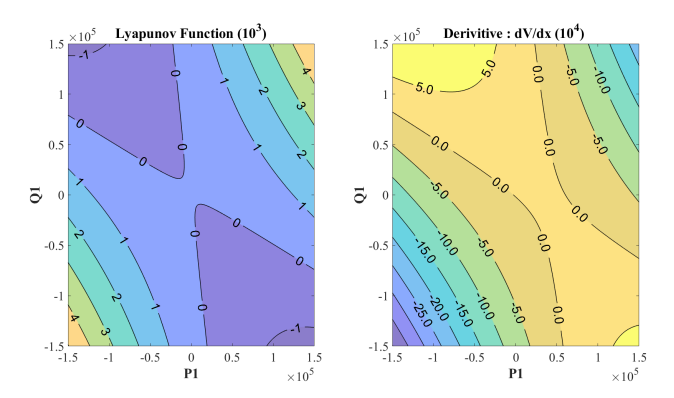


Fig. 3. Lyapunov function based on SOS (left) Derivative of Lyapunov function based on SOS (right).

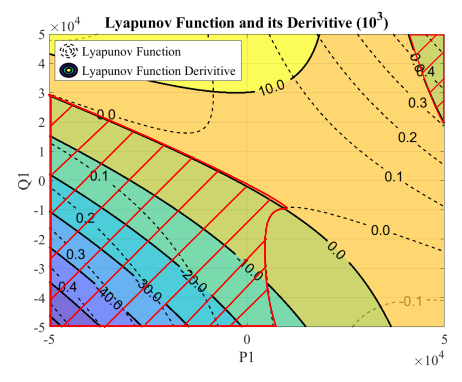


Fig. 4. The stability region satisfied the Lyapunov stability conditions.

## C. Sensitivity Analysis

The following section represents the effect of two scenarios including a load-changing event and control modification on the stability region. These two scenarios are common in inverter-based microgrids as a smart system to modify the system based on the transient and permanent changes and guarantee reliable and stable operation.

- 1) Load Changing: Load reconfiguration is a remedy to increase the system reliability during contingencies, resulting in a change in the stability region. Appropriate load reconfiguration or load shedding enlarges the region of stability, improving the stability capability of the network during the possible transient fault in the future. Fig. 5 illustrates the impact of load increasing in the stability region. By increasing load 1, the contour lines for the same V-slices shrink to a smaller region of stability.
- 2) Control Modification: Various inverter controlling techniques are applied on the inverter switching system to guarantee a reliable and stable operation. Changing the controlling

$$\mathbf{A_{Microgrid}}(\mathbf{X_{Microgrid}}) = \begin{bmatrix} A_{IBR} + B_{IBR}R_vM_{IBR}C_{IBR_c} & B_{IBR}R_vM_{Ntwrk} & B_{IBR}R_vM_L \\ B_{Ntwrk}R_vM_{IBR}C_{IBR_c} & A_{Ntwrk} + B_{Ntwrk}R_vM_{Ntwrk} & B_{Ntwrk}R_vM_L \\ B_{load}R_vM_{IBR}C_{IBR_c} & B_{load}R_vM_{Ntwrk} & A_{load} + B_{load}R_vM_L \end{bmatrix}$$
(22)

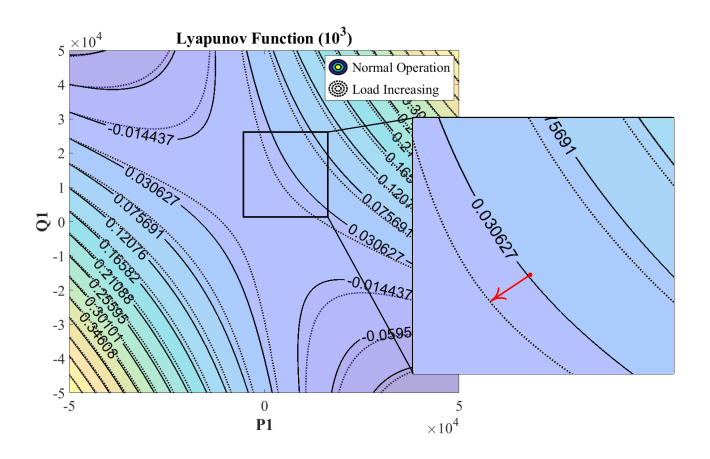


Fig. 5. (a) Increasing load.

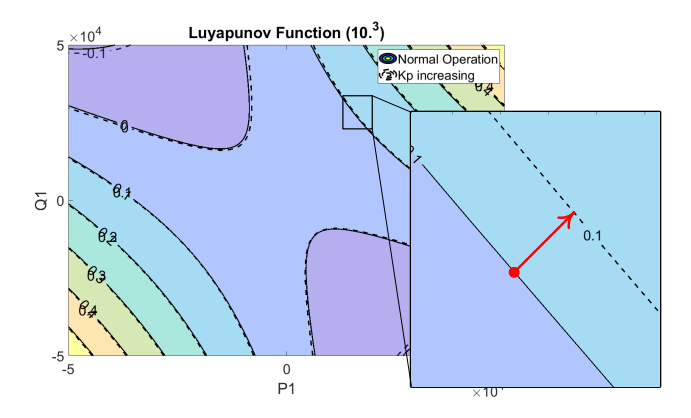


Fig. 6. (a) Increasing Kpv.

parameter during contingencies or normal operation is the nature of a smart controlling system. Besides all controlling objects for making an appropriate decision for the switching system, the region of attraction can be another criterion for modifying the controlling parameter. Fig. 6 represents the effect of increasing the  $K_{pv}$  on the region of stability, leading to expanding the contour lines of the stability region and improving the stability capability of the system.

### V. CONCLUSION

This paper has presented a sum of squares method to construct the domain of attraction for the large-signal stability analysis of inverter-based microgrids. The nonlinear dynamic model has been developed for a grid-connected microgrid. The results proved that the SOS-based Lyapunov method could construct a less conservative domain of attraction for stability analysis, determining a more precise critical clearing time compared to the domain constructed by Krasovskii's method.

However, the computational process of the sum of squares method for a high-order state space model was extremely time-consuming, and in some cases, could not converge to a reasonable response. In SOSTOOL, a major problem with using higher-degree Lyapunov functions for a large-scale system was the significant increase in the number of optimization decision

variables. As a solution to take the advantage of the SOS-based method for a larger-scale system, a simpler and small-order model of inverters should be applied.

The simple dynamic model must have reasonable approximations for transient stability analysis. One of the acceptable and accurate models of inverters is the 5-order state-space model of inverter-based resources proposed by [13]. The other low-order state space model is the synchronverter model [8]; however, the synchronverter model can provide only frequency and angle as the states. Therefore, there is a trade-off between the number of states that can be monitored and the feasible computation process.

On the other hand, although Krasovskii's method is not accurate enough, this is more salable and the computation time is acceptable for a complex system in terms of the numbers of inverter-based resources and distributed generators.

#### ACKNOWLEDGEMENT

This material is based upon work supported by the U.S. National Science Foundation under Grant ECCS-2033927.

#### REFERENCES

- A. Khodaei, S. Bahramirad, and M. Shahidehpour, "Microgrid planning under uncertainty," *IEEE Transactions on Power Systems*, vol. 30, no. 5, pp. 2417–2425, 2014.
- [2] M. Mansour-lakouraj and M. Shahabi, "Comprehensive analysis of risk-based energy management for dependent micro-grid under normal and emergency operations," *Energy*, vol. 171, pp. 928–943, 2019.
- [3] Z. Shuai, Y. Sun, Z. J. Shen, W. Tian, C. Tu, Y. Li, and X. Yin, "Microgrid stability: Classification and a review," *Renewable and Sustainable Energy Reviews*, vol. 58, pp. 167–179, 2016.
- [4] S. Wang, J. Su, X. Yang, Y. Du, Y. Tu, and H. Xu, "A review on the small signal stability of microgrid," in 2016 IEEE 8th International Power Electronics and Motion Control Conference (IPEMC-ECCE Asia). IEEE, 2016, pp. 1793–1798.
- [5] M. Kabalan, P. Singh, and D. Niebur, "A design and optimization tool for inverter-based microgrids using large-signal nonlinear analysis," *IEEE Transactions on Smart Grid*, vol. 10, no. 4, pp. 4566–4576, 2018.
- [6] D. Marx, P. Magne, B. Nahid-Mobarakeh, S. Pierfederici, and B. Davat, "Large signal stability analysis tools in dc power systems with constant power loads and variable power loads—a review," *IEEE Transactions* on *Power Electronics*, vol. 27, no. 4, pp. 1773–1787, 2011.
- [7] H. Hosseinpour, M. MansourLakouraj, M. Ben-Idris, and H. Livani, "Lyapunov-based large-signal stability analysis of inverter-based microgrids," in 2022 North American Power Symposium (NAPS). IEEE, 2022, pp. 1–6.
- [8] F. Andrade, K. Kampouropoulos, L. Romeral, J. C. Vasquez, and J. M. Guerrero, "Study of large-signal stability of an inverter-based generator using a lyapunov function," in *IECON 2014-40th Annual Conference of the IEEE Industrial Electronics Society*. IEEE, 2014, pp. 1840–1846.
- [9] W. Tan and A. Packard, "Stability region analysis using sum of squares programming," in 2006 American Control Conference. IEEE, 2006, pp. 6–pp.
- [10] N. Pogaku, M. Prodanovic, and T. C. Green, "Modeling, analysis and testing of autonomous operation of an inverter-based microgrid," *IEEE Transactions on power electronics*, vol. 22, no. 2, pp. 613–625, 2007.
- [11] P. A. Parrilo, "Polynomial games and sum of squares optimization," in *Proceedings of the 45th IEEE Conference on Decision and Control*. IEEE, 2006, pp. 2855–2860.
- [12] A. Papachristodoulou, J. Anderson, G. Valmorbida, S. Prajna, P. Seiler, and P. A. Parrilo, SOSTOOLS: Sum of squares optimization toolbox for MATLAB, 2013, available from http://www.mit.edu/~parrilo/sostools.
- [13] M. Kabalan, P. Singh, and D. Niebur, "Nonlinear lyapunov stability analysis of seven models of a dc/ac droop controlled inverter connected to an infinite bus," *IEEE Transactions on Smart Grid*, vol. 10, no. 1, pp. 772–781, 2019.